European Review for Medical and Pharmacological Sciences 2021; 25: 5769-5780

A radiomics method based on MR FS-T2WI sequence for diagnosing of autosomal dominant polycystic kidney disease progression

L. CONG[1], Q.-Q. HUA[2], Z.-Q. HUANG[2], Q.-L. MA[3], X.-M. WANG[2], C.-C. HUANG[4], J.-X. XU[4], T. MA[2]

[1]Department of Interventional Ultrasound, Shandong Medical Imaging Research Institute, Cheeloo College of Medicine, Shandong University, Jinan, China
[2]Department of Radiology, Shandong Provincial Hospital Affiliated to Shandong University, Jinan, China
[3]Department of Radiology, Tai'an City Central Hospital, Taian, China
[4]Department of Research Collaboration, Beijing Deepwise & League of PHD Technology Co., Ltd, Beijing, China

Lin Cong and Qianqian Hua contributed equally to this work

Abstract. – OBJECTIVE: We aimed to construct/validate a radiomics method based on MR FS-T2WI sequence for the evaluation of kidney function in patients with autosomal dominant polycystic kidney disease (ADPKD).

PATIENTS AND METHODS: The clinical data and MRI images of 114 patients with ADPKD were retrospectively analyzed. With a glomerular filtration rate of 60 mL/min per 1.73 m2 as the cutoff value, patients were divided into two groups, where there were 59 patients with GFR ≥60 mL/min per 1.73 m^2 (including CKD1 and CKD2 phase) and 55 patients with GFR <60 mL/min per 1.73 m^2 (including CKD3 phase and higher). All patients underwent the 3.0T MR scan of the kidney. Then, the kidney were delineated layer by layer based on the FS-T2WI sequence to obtain the volume of interest (VOI) for radiomics features extraction. The optimal radiomics features were selected by least absolute shrinkage and selection operator (LASSO). Three kinds of data modality including the pure clinical data, the pure image data and the clinical-image fused data were utilized to establish three types of models (clinical, image and with their combination) separately by five machine learning classifiers: k-nearest-neighbors (KNN), support vector machine (SVM), logistic regression (LR), random forests (RF) and multi-layer perception (MLP). Receiver operating characteristic (ROC) curve, areas under the curve (AUC), sensitivity, specificity and precision were employed to evaluate the model's effectiveness to diagnosis the glomerular filtration rate of patients with ADPKD based on different models. Besides, Delong test was applied to compare ROCs between models.

RESULTS: 960 radiomics features were extracted from each VOIs, and clinical information included the gender and age of each patient. After feature selection, 23 and 21 features based on pure image data and clinical-image fused data were independently used to construct models for the kidney function evaluation. The clinical-image fused model (AUC=0.89) has better performance than the pure image model (p=0.046) and pure clinical model (p<0.001). Clinical-image fused model based on LR classifier showed the best diagnostic efficiency, with AUC=0.89, sensitivity=0.8867 and specificity=0.7959.

CONCLUSIONS: The MR FS-T2WI radiomics analysis based on clinical-image fused model is instrumental in evaluating and predicting the kidney function of patients with polycystic kidney disease.

Key Words:
Autosomal dominant polycystic kidney disease, Magnetic resonance imaging, Radiomics, Kidney function.

Introduction

Autosomal dominant polycystic kidney disease (ADPKD) is the most common hereditary renal cystic disease, the prime manifestations of which are vesicles in varied dimensions diffusing and distributing both kidneys, often involving tissue and organs, such as the liver, spleen and

Corresponding Author: Teng Ma, MM; e-mail: 201957000591@email.sdu.edu.cn

cerebral arteries. The formation and dimension enlargement of progressive renal cysts will destroy the structure and function of kidneys, and eventually result in end-stage renal disease. End-stage renal disease is recognized as one of the four major disease leading to renal failure[1], from which there are 12.5 million people are suffering around the world[2]. Precise clinical evaluation on renal function plays a critical part in prognosis for patients with polycystic kidney disease. Serum creatinine level (Scr) and estimated glomerular filtration rate (eGFR) are two popular indices in clinical monitoring of ADPKD renal function. Estimated GFR, however, does not change until the later phase of diseases due to compensatory glomerular hyperfiltration[3], thus constraining its exercise in advanced diseases[4]. In recent years height-adjusted total kidney volume (htTKV) is considered to be another biological indicator available for identifying the progression of polycystic kidney disease[5,6]. However, its universal applicability remains controversial in terms of the diagnostic potency for middle and advanced patients and the efficacy of drugs[7,8]. MRI holds a significant superiority in polycystic kidney disease diagnosis. Its routine sequences are so clear as to present the location, morphology, internal ingredients and density of cysts, and the condition of residual renal parenchyma. Also, MRI provides multi-functional imaging sequences and quantitative techniques[9-11], such as diffusion weighted imaging (DWI), intra-voxel incoherent motion (IVIM) and blood oxygen level dependent (BOLD), to closely observe the changes in renal structure. As the advancement of precision medicine, the use of high throughput to extract quantitative information from medical images comes to the foreground. MRI image-based radiomics analysis shows a better performance in quantizing image information. It cannot only unearth potential image information naked eyes cannot discern but also reflect pathological changes of VOI[12]. Routine MRI radiomics analysis are gradually being applied to diagnosis and treatment for major visceral diseases of abdominal and pelvic cavities, including liver tumor and rectal cancer[13,14]. In contrast, its practice in polycystic kidney disease is barely reported. This study, by extracting the omics features of FS-T2WI sequence images from patients with polycystic kidney disease and multivariate analysis, aims to establish a machine learning model useful for diagnosis and prediction of the polycystic kidney disease progression.

Patients and Methods

Patients

This study was approved by the Ethics Committee of Shandong Provincial Hospital Affiliated to Shandong University. Signed written informed consents were obtained from all participants before the study. 114 patients with polycystic kidney disease, who received outpatient diagnosis and hospitalization diagnosis and treatment in our hospital from January 2017 to June 2019, were given retrospective analysis. Of these patients, 54 were males and 60 were females, aged between 24 and 75 years old, with an average of 49.11±9.85 years old. Chronic kidney disease (CKD), according to the US clinical practice guidelines for chronic kidney disease and dialysis (NKF-K/DOQI), were divided into 5 stages. With a glomerular filtration rate of 60 mL/min per 1.73 m^2 as the division boundary, these patients were divided into two groups. One group contained 59 patients with a GFR $\geq$ 60 mL/min per 1.73 m^2 (including CKD1 and CKD2 stages), and the other grouped 55 patients having a GFR $<$ 60 mL/min per 1.73 m^2 (including CKD3 and more advanced stages). The inclusion criteria were as follows: (1) all patients had had routine MRI examination including FS-T2WI sequence before treatment; (2) there were no artifacts that may impact image texture analysis; (3) and glomerular filtration rate examination should be implemented before treatment and no longer than 72 h from MRI examination. Meanwhile, the exclusion criteria referred to patients (1) with MRI contraindications and (2) with a blurred boundary between renal lesion and surrounding structures.

Examination Methods

All patients were given routine renal MRI plain scanning. The scanning adopted Siemens 3.0T MRI scanner to perform with supine position and head-first position, and 8-channel abdominal phased array coil (Magnetom Verio, Siemens, Erlangen, Germany) to receive signals and covered the whole kidneys. Before the scanning, fasting time was required and kept for 6-8 h. The transversal axial image T2WI employed breath-triggered fat suppression FSE sequence. Scanning parameters included TR 2000-6000 ms, TE 80-104 ms, echo train length 8-16, matrix 320-224, thickness 6 mm, inter-layer space 0.6 mm, and field of vision 36 cm × 36 cm – 40 cm × 40 cm.

Image Annotations

All the patient FS-T2WI images were exported in "*.DICOM" from picture archiving and communication system (PACS) and uploaded to the Dr. Wise Multimodal Research Platform (https://research.deepwise.com) (Beijing Deepwise & League of PHD Technology Co., Ltd, Beijing, China) for radiomics analysis, including image annotation and feature extraction.

The radiomics analysis process was shown in Figure 1.

Two medical practitioners with 10-year practical experience of imaging diagnosis were invited to operate the software and interpret images. For the region where the two doctors stood with different views, exchange discussion was so necessary as to reach an agreement. Four image outline approaches were involved as shown below. (1) Instead of a specific division on each cyst, all the renal lesions were viewed as a whole and outlined. (2) Except for the newly emerged layer and the about-to-disappear layer of a focus, all the contour layers of a kidney were given ROI outlining to acquire renal volume of interest (VOI). (3) Semi-automatic outlining was applied. The outlining software equipped in the radiomics platform could automatically identify the rough contour of a lesion. Where the outlining effect was not satisfactory, manual adjustment was available. (4) If necessary, the interactive viewer mounted in the outline software may be opened to localize in combination with sagittal and coronal images.

Characteristic Extraction

Original MR images should be pre-processed by a high-throughput or low-throughput wavelet filter and Laplace-Gaussian filter with different λ parameters for 8 wavelet-preprocessed images and 5 images pre-processed by Laplace-Gaussian filter. From the original MR images and the preprocessed images were extracted radiomics features, including the first order features of pixel value of the images, the morphological features

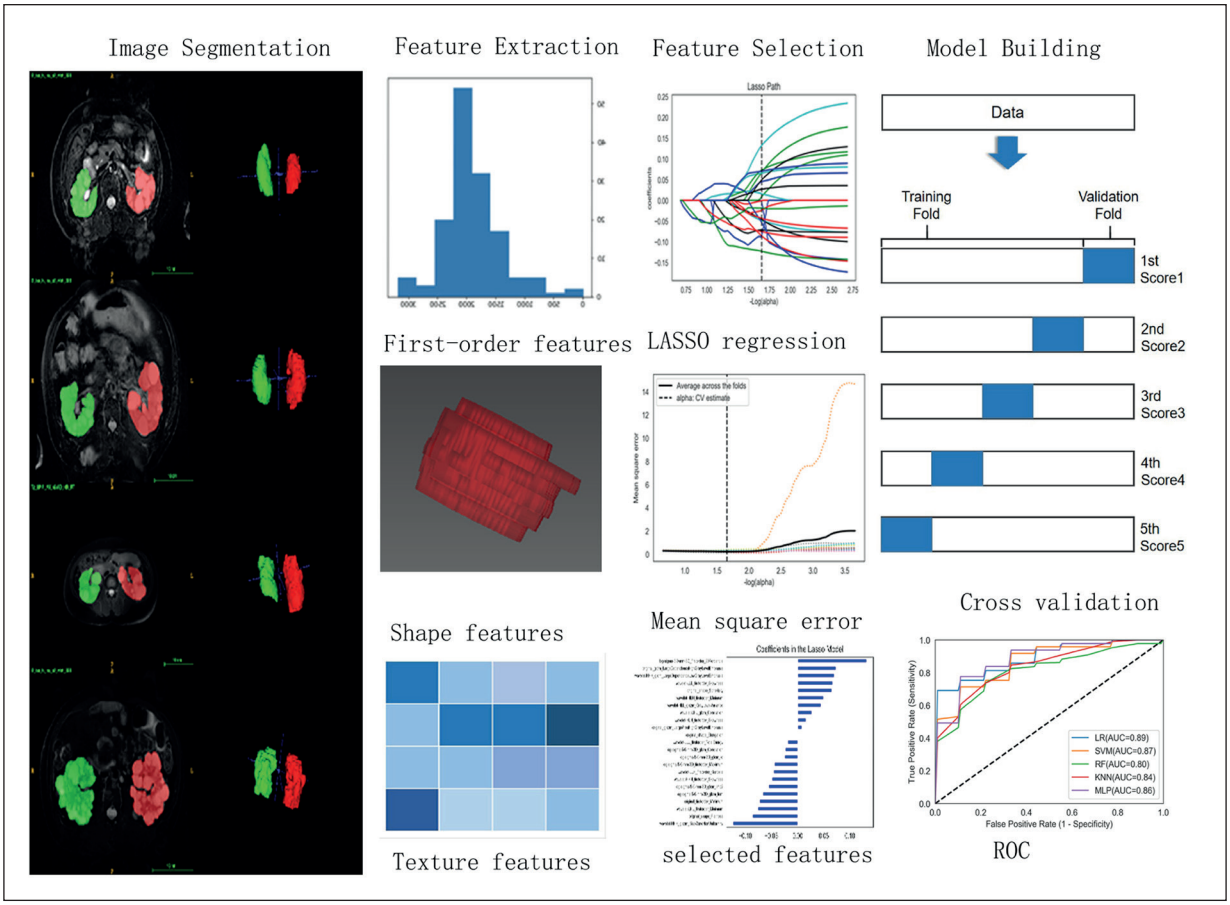

Figure 1. The flow chart of radiomics process.

describing the morphology of a tumor, as well as the texture features of gray level cooccurrence matrix (GLCM), gray level run length matrix (GLRLM), gray level size zone matrix (GLSZM) and gray level dependence matrix (GLDM) used to describe the internal and external texture of a tumor. From each lesion 960 radiomics features were extracted in total for Z-score standardization (i.e. the value was subtracted from the mean and then divided by the standard deviation). LASSO (Least Absolute Shrinkage and Selection Operator) algorithm was applied at last for feature dimension reduction and feature selection. The method apply a shrinking (regularization) process where it penalizes the coefficients of the regression variables shrinking some of them to zero. During features selection process the variables that still have a non-zero coefficient after the shrinking process are selected to be part of the model. The goal of this process is to minimize the prediction error.

Model Construction

The study, in view of different types of data modality, three types of models (clinical, image and with their combination) were respectively constructed by five machine learning classifiers to diagnose and determine the progression of polycystic kidney disease. The five machine learning classifiers were included: k-nearest-neighbors (KNN), support vector machine (SVM), logistic regression (LR), random forests (RF), multi-layer perception (MLP). Each model was built by 5-fold cross validation strategy, evaluated with receiver operating characteristics (ROC) curve, areas under the curve (AUC), sensitivity, specificity and precision. The ROCs of every two models were compared using Delong test.

Statistical Analysis

The machine learning classifiers were structured by Scikit-learn software package (Version 0.20.3); ROC curves were drawn with Matplotlib (Version 3.1.0). Delong test was performed by software MedCalc (Version 19.0.2). $p<0.05$ was considered to be statistically significant.

Results

Radiomics Features Analysis

This study attached the focus on the original images and extracted through wavelet transform 960 imaging features that included 198 first-order features, 14 shape features and 748 texture features. The clinical information of each patient includes gender and age. The clincial-image fused data required the 960 original radiomics features and 2 clinical information for further analysis. Feature selection and reduction were completed by LASSO. From pure imaging data, key relevant features were selected and acquired by 5-fold cross validation. As shown in the Diagram of LASSO Mean Square Error Path (Figure 2), the dotted lines in different colors together represent that each group of cross validation samples corresponds a specific –log (alpha) and comes to a distinct square error. The black solid line denotes the mean of ten groups of square errors. An optimal alpha refers to the one where the mean square error reaches to the lowest. The optimal alpha obtained here was 0.02206 while the -log(alpha) was 1.65647. In the Diagram of Coefficient Solution Path (Figure 3)

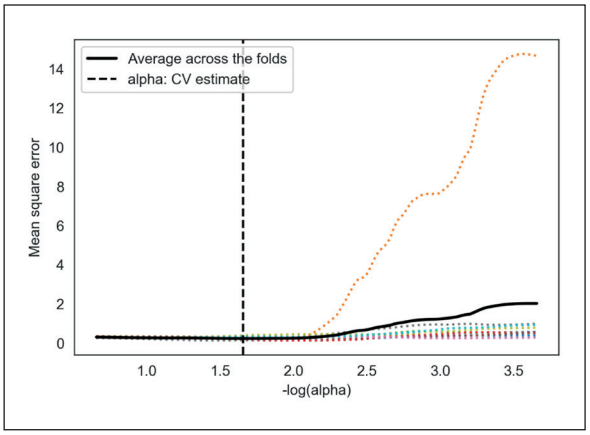

Figure 2. Diagram of imaging data LASSO square error path.

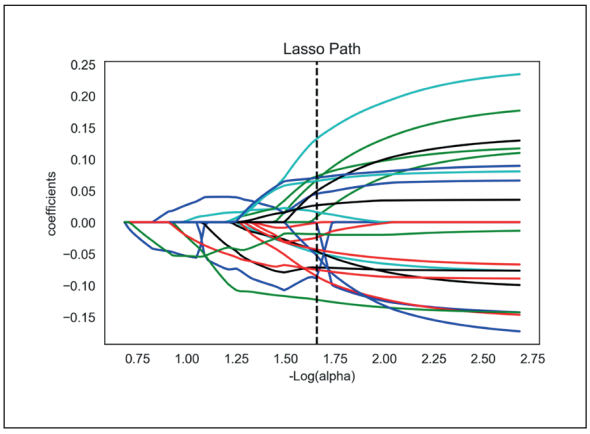

Figure 3. Diagram of imaging data coefficient solution path.

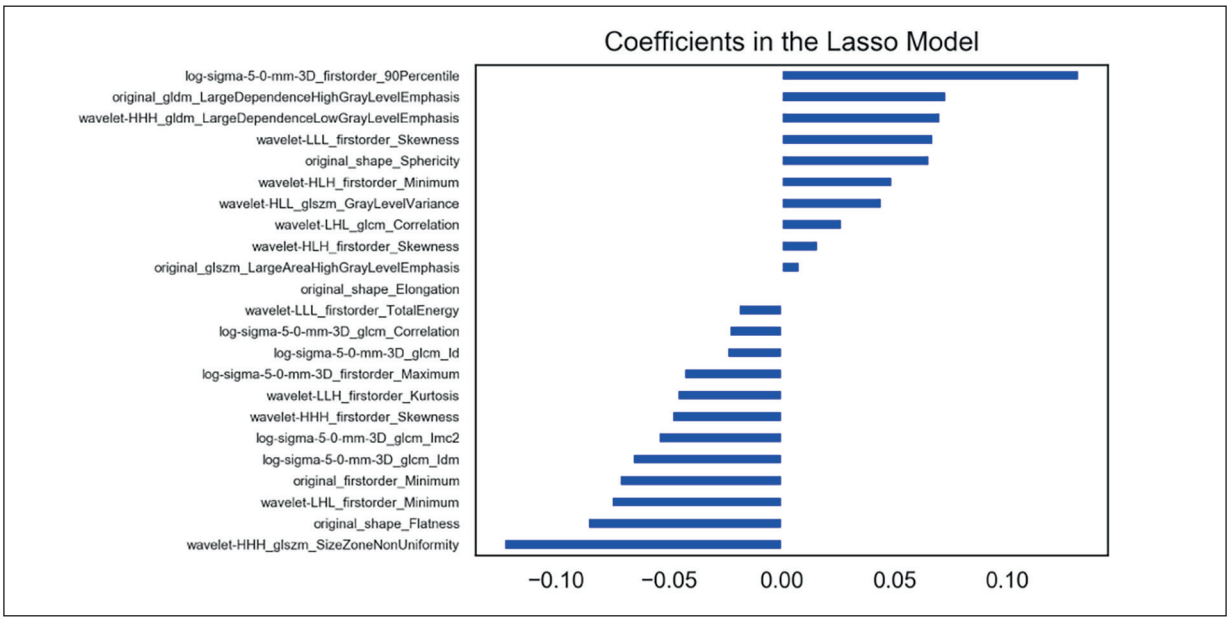

Figure 4. 23 radiomics features screened by imaging data dimension reduction and their corresponding characteristic coefficients.

the longitudinal axis stands for the coefficient of each features in the LASSO model. These coefficients change with the values of alpha. Thanks to the correspondence, it is feasible to discover the coefficient of a characteristic in view of the optimal alpha. Given that features with a non-zero coefficient were selected, 23 features of clinical significance were eventually selected, included 6 features extracted through the original images, 11 features processed by wavelet transform, and 6 features treated with Laplace transform; 10 first-order features, 3 morphological features and 10 texture features (Figure 4).

From the clinical-image fused data were acquired with an optimal alpha of 0.02365 and a –log (alpha) of 1.62617. The diagrams of LASSO square error path and coefficient solution path are shown as Figure 5 and Figure 6. After dimension reduction, from the 960 original features 21 ones with clinical significance were selected, including 5 extracted by original images, 9 through wavelet transform and 6 through Laplace transform; or 8 first-order features, 2 morphological features and 10 texture features, together with the age information of each patient (Figure 7).

Machine Learning Model Evaluation

Three types of models (clinical, image and with their combination) were built by five classifiers including LR, SVM, RF, KNN, as well as MLP. Results of predictive performance (AUC, sensitivity, specificity, and accuracy) is summarized in Table I.

Figure 8 illustrates the diagnostic potency of LR model on the function of kidneys infected by polycystic kidney disease under different data modality. To compare and determine whether machine learning models can differ from each other, the ROC curve of each model were given DeLong test (Table II). Take LR classifier as an example, the differences between three models under different data were compared. The clini-

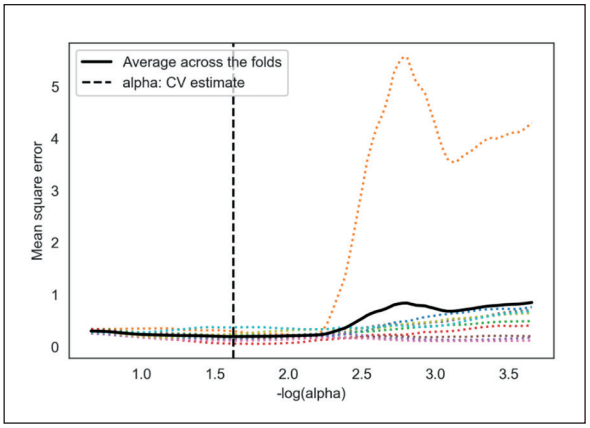

Figure 5. Diagram of clincial-image fused data LASSO square error path.

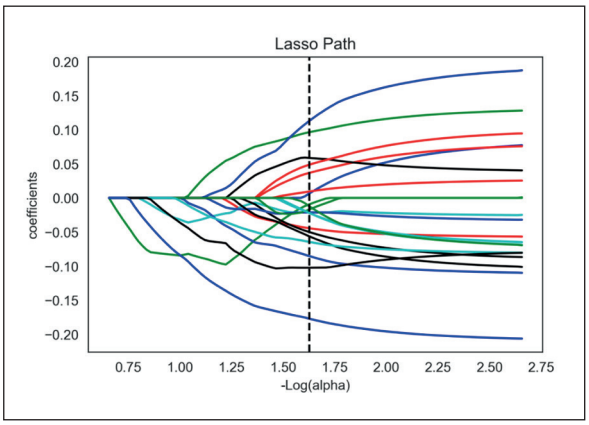

Figure 6. Diagram of clincial-image fused data coefficient solution path.

cal-image fused model (AUC=0.89) showed an improved performance over the pure image model (p=0.046) and pure clinical model (p<0.001). Regard the other 4 machine learning models, the clinical-image model demonstrated a more satisfactory effect than pure image model, but without a statistically significant difference (p>0.05), whereas showed a significantly superior effect than pure clinical model (p<0.05).

To study the diagnostic potency of the model built with clinical-image fused data, the diagnostic efficacy of different classifiers on the renal function infected by polycystic kidney disease were compared. Their ROC curves are shown in Figure 9. DeLong test indicated the presence of a statistical difference between LR model and RF model (p=0.0087), and an absence of obvious difference between the other 4 models (SVM, RF, KNN and MLP).

The study investigated the potency of different classifiers to diagnose the renal function infected by polycystic kidney disease under image model. Their ROC curves are shown in Figure 10. Through DeLong test, the MLP model was found to have the maximum AUC of 0.85, indicating that it held the best diagnostic potency. Between the RF model and the MLP model a significant statistical difference (p=0.0226) was noted, so was between the RF model and the KNN model (p=0.0328), while no remarkable difference was found between other models.

The image data clinical fusion model, built by LR to evaluate renal function, presenting an AUC of 0.89, sensitivity of 0.8667 and specificity of 0.7959, considered to possess the best diagnostic potency. Among image models, the MLP model reached the optimal diagnostic potency with a performance of 0.85 in AUC, 0.8222 in sensitivity and 0.7347 in specificity.

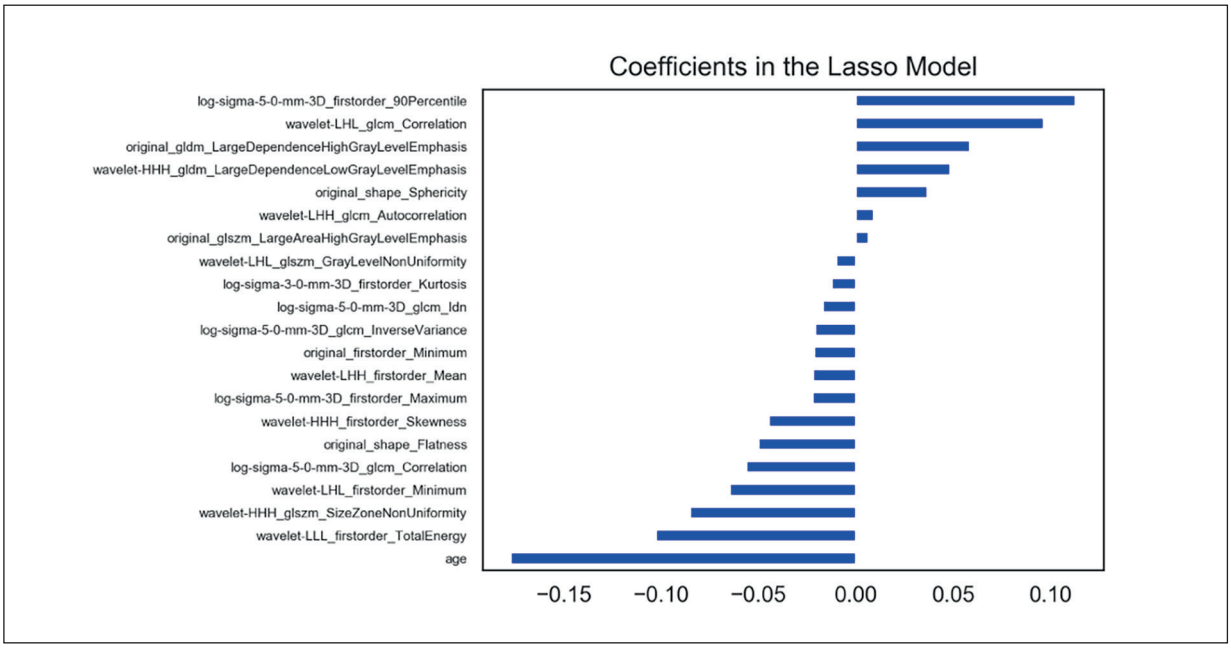

Figure 7. 21 radiomics features Screened by Clincial-image Fused Data Dimension Reduction and their Corresponding Characteristic Coefficients.

Table I. Performances of clinical, image, combined clinical and image models.

	Classifier	AUC	Sensitivity	Specificity	Precision
Clinical model	LR	0.67 ± 0.09	0.8222	0.4694	0.6383
	SVM	0.62 ± 0.10	0.6889	0.5306	0.6064
	RF	0.67 ± 0.10	0.8444	0.4490	0.6383
	KNN	0.60 ± 0.10	0.9556	0.2653	0.5957
	MLP	0.57 ± 0.10	0.5556	0.7551	0.6596
Image model	LR	0.83 ± 0.07	0.7111	0.8163	0.7660
	SVM	0.84 ± 0.07	0.8222	0.7959	0.8085
	RF	0.74 ± 0.08	0.8889	0.5102	0.6915
	KNN	0.83 ± 0.07	0.7111	0.7959	0.7553
	MLP	0.85 ± 0.07	0.8222	0.7347	0.7765
Fused model	LR	0.89 ± 0.06	0.8667	0.7959	0.8298
	SVM	0.87 ± 0.06	0.8888	0.7959	0.8404
	RF	0.80 ± 0.08	0.9111	0.5714	0.7340
	KNN	0.84 ± 0.07	0.6667	0.8776	0.7767
	MLP	0.86 ± 0.06	0.8222	0.8571	0.8404

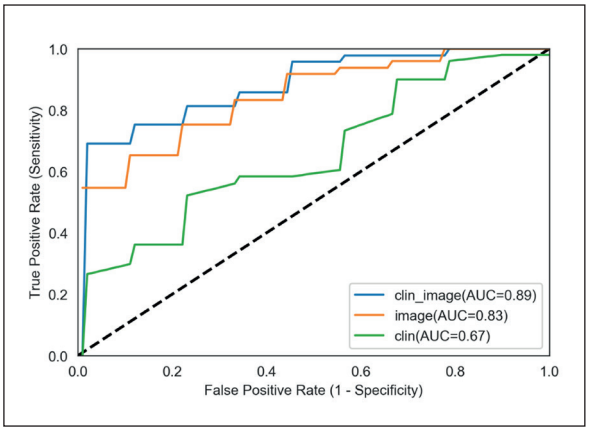

Figure 8. ROC Curves of LR Model of Different Data Modalities (clin-image: model of imaging features and clinical information; image: model of imaging features alone; clin: model of clinical information alone).

Discussion

In recent years, with the development of artificial intelligence, radiomics technology has become a research focus in the field of medical imaging.. Using mathematical and statistical methods, radiomics analysis analyzes the gray distribution features of pixels in images, extracts from the images the radiomics features (including first-order features, shape features and texture features) not recognizable for human eyes, and at last, in a quantitative way, described these radiomics features acquired. This technique, thanks to its prevention from the effect of subjective factors and professional levels of medical practitioners, could be working as a remedy for the defects lying in routine examinations and imaging[15]. It has been applied to diagnoses of multiple viscera organs and various diseases[16-18], but remains rare in the studies on polycystic kidney disease. Height-adjusted TKV though globally recognized as a reliable indicator to reflect the renal function infected by polycystic kidney disease[2,19,20]. Some studies demonstrate that its growth speed lacks a correlation with the weakening of renal function[21,22], and the indicator itself can only reflect the size of kidneys, indicate the overall progression of diseases, but not provide more information related to renal tissue and structure in MRI or CT images[23]. Resorting to the difference in T2

Table II. Data modalities and statistical differences between machine learning models.

	Clinical + image data *vs.* image data	Clinical + image data *vs.* clincal data	Image data *vs.* clincal data
LR	0.0466	0.0002	0.0174
SVM	0.4013	0.0002	0.0019
RF	0.3028	0.0492	0.3309
KNN	0.7259	0.0004	0.0002
MLP	0.7616	< 0.0001	0.0001

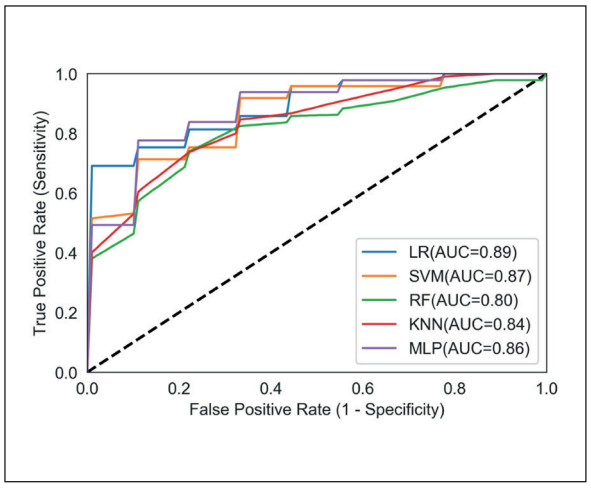

Figure 9. Performances of different classifiers for clinical-image fused data.

between tissue, MRI FS-T2WI sequence can not only clearly displays the morphology of lesions but also embody the pathological features of diseased tissue. This sequence well performs in distinguishing liquid-filled cysts (high signal intensity) from renal parenchyma (low signal intensity). It thus holds an evident superiority in diagnosing diseases which are characterized and manifested by progressive polycystic disease, for example, autosomal dominant polycystic kidney disease (ADPKD)[24]. Furthermore, the addition of inter-tissue contrast ratio enables images to contain more radiomics features with meaningful in the differentia diagnosis[25]. As early as 2016, the ERA-EDTA WGIKD/ERBP statement has recommended MRI examination to clinical practice for diagnosis of ADPKD patients' fast advancement phases[26]. By the aid of radiomics

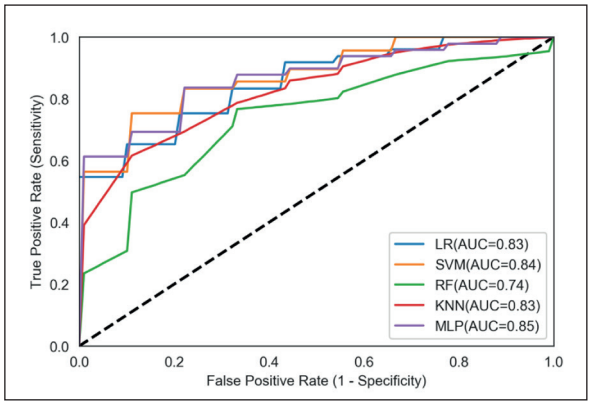

Figure 10. Performances of different classifiers for image data.

analyzing techniques, we are now able to collect from MRI images a great many quantitative indicators, such as grayscale distribution, inter-voxel spatial relationships and texture heterogeneity. Meanwhile, these indicators are enabled to reflect in a more accurate way the heterogeneity and micro information inside diseased parts[27]. The study is designed to explore and discuss whether radiomics techniques can take the credit of being a new means to reflect the progression of polycystic kidney disease; to analyze the potency of diagnosing disease progression of three modalities (pure image data based modality, pure clinical data based modality and clinical-image fused data based modality) and of five machine learning models (k-nearest-neighbors (KNN), support vector machine (SVM), logistic regression (LR), random forests (RF), multi-layer perception (MLP).

960 radiomics features were extracted from original images and acquired through wavelet transform and Laplace transform. However, on account of the possible presence of irrelevance and redundancy in these features, LASSO was then adopted to reduce their dimension and screen them. LASSO has, so far, been mainly applied to linear models. Its essence is to add a penalty function on the basis of residual sum of squares. In this penalty function, a tune parameter alpha was employed to weigh the balance between the effects of analogous fitting and penalty items, with an aim to avoid model over fitting while to minimize classification errors. The tune parameter alpha was chosen through five-fold cross validation. In view of its value were obtained valuable, incorporable parameters and their relevant regression coefficients. These parameters included in models were thereby left better repeatability, which had the collected radiomics features more stable.

It is a common ending for ADPKD patients to have a CKD characterized by weakened renal function. The study results indicated a significantly better potency of clinical-image fused data-based model than that of both models based on pure clinical data and pure image data in differentiating the function of polycystic kidney disease infected kidneys, differentiating the renal function with an eGFR $\geq$ 60 mL/min per 1.73 m^2 (including CKD1 and CKD2 phases) from the other with an Egfr < 60 mL/min per 1.73 m^2 (including CKD3 and advanced phases). By LASSO dimension reduction on clinical-image fused data, from the 960 original features, 21

clinically meaningful features were screened out, covering 8 first-order features, 2 morphological features and 10 texture features, as well as the age information of patients. Radiomics analysis ascribes its superiority to its capability of integrating morphological features of kidneys, such as the dimension, number and spatial distribution of cysts, the growth of an individual cyst, as well as the asymmetry of cyst distribution, and of extracting strongly related characteristic parameters to reflect the morphological changes and tissue composition status of kidneys, while not demanding separate division and classification on these cysts. Of the study results, the flatness and phericity embodied the curvature changes in renal contour and the regularity of its overall shape. Total energy and 90th percentile took the biggest weight among the first-order features. They reflected the smoothness of grayscale distribution and the roughness of texture, thus being viewed as the measurement of tissue homogeneity[23]. The more complex the lesions, the lower the total energy. The overall lesion of a diseased kidney was outlined. Its internal cysts were distributed mainly in three patterns: multiple macro-cysts, partial cysts and dense microcysts. Each distribution pattern produced oppression on its nearby renal parenchyma as the cyst size enlarged and the cyst number increased. The oppression induced regional ischemia, which furthermore impaired renal function. Normal renal tubules were then blocked, and eventually, progressive renal function failure was triggered[28]. Therefore, the ratio of cystic part to residual renal parenchyma was considered to be an important factor in determining the renal function of patients. Thought the heterogeneity of diseased internal compositions is hard for human eyes to judge on images, texture analysis enables the discovery of objective information of tissue composition from conventional images.

The study, utilizing clinical-image fused data, screened out 10 advanced-order texture features with clinical significance, including gray level co-occurrence matrix (GLCM), gray level size zone matrix (GLSZM) and gray level dependence matrix (GLDM). These features reflected the spatial correlation of image gray levels[29]. The size-zone non-uniformity (SZN), correlation, large dependence low gray level emphasis (LDLGLE) and large dependence high gray level emphasis (LDHGLE) embodied the disorder degree of renal structure, the scattering degree of cysts, the signal changes resulted from the differences in cyst compositions (pure cyst fluid, bleeding, protein included and co-infection), as well as the differences in brightness of peripheral structures. Kline et al[23] added the 3 kinds of ADPKD image texture features screened into the model devised to predict the renal function of ADPKD patients by age, eGFR and htTKV. The sophisticated model heightened the correlation between prediction models and the deterioration of renal function. Texture features can provide information that other non-image-based clinical indicators (such as renal volume and glomerular filtration rate) cannot provide. They were thus proven to a powerful supplement to extant diagnostic indicators.

The study also selected and included the age and gender of patients as additional information. Previous studies demonstrate the availability of age and total kidney volume (TKV) being indicators of predicting ADPKD disease progression[6]. Recently, the U.S. Food and Drug Administration and the European Medicines Agency included these two indicators, employing them as prognostic imaging biomarkers for ADPKD research and clinical trials[23]. By investigating the clinical-image fused data-based modality, we found that age occupied the dominant weight among the 21 features we screened out. This suggested an important clinical role of age in determining the decrease of renal function in patients with polycystic kidney disease. The elder population showed, in general, a lower glomerular filtration rate.

Besides different data modalities, we also studied the diagnostic potency of multiple data models on the progression of polycystic kidney disease. For models constructed with clinical-image fused data, LR model won the best diagnostic potency, with a 0.89 AUC, a 0.8667 sensitivity and a 0.7959 specificity. Comparatively, MLP model peaked among models set up with pure image data; it reached 0.85 in AUC, 0.8222 in sensitivity and 0.7347 in specificity. The LR model is one of the algorithms that are most frequently used for binary classification tasks. It is categorized as a supervised machine learning model, widely popular in terms of application[30]. It is mostly utilized to address a regression or classification problem. With an assumption that data obey Bernoulli distribution, the model employs gradient descent to optimize parameters by maximizing the likelihood function and adopts a simple model to achieve data dichotomy. LR model holds a strong explanatory power. MLP is a feed-forward supervised neural network. It

determines the non-linear mapping from an input to an output by parameterizing a set of network weights. In this study, LR and MLP were involved in machine learning with different data. Both attained the best diagnostic performance separately under clinical-image fused data-based and pure image data-based modalities.

The novelty of this study is that radiomics technology is validated as a new effective method to reflect the autosomal dominant polycystic kidney disease progression. Radiomics technology extracts differences in signals that we cannot sense visually from FS-T2WI images, not only makes full use of but also increases the information given by the conventional MRI images, and provides quantifiable parameters of renal tissue structure. It can be viewed as an effective supplement to traditional biological markers and clinical information. In this study, we mainly explored the feasibility and diagnostic efficacy of radiomics technology in the application of ADPKD, all patients were divided into only two groups. Based on the results of this study, we believe that it is possible with this method to control renal function in different times. Then, the focus of the following work will be to classify the patients according to the CKD staging criteria, and to further study the diagnostic and predictive ability of radiomics technology for evaluation renal functions at different times and at different stages of ADPKD. Renal function in all patients was followed up every 6 months. In the following research, the ability of radiomics technology to predict subsequent progression to CKD stage 3 and significant reduction in GFR will be also mainly assessed.

Despite the above-mentioned superiorities, the study still holds some limitations[1]. The study is a retrospective research. Its sample scale is small; thus, there may be biases. Further analyses are required to conduct by prospective studies with a large sample[2]. Because, ROI is semi-automatic outlining, it may harbor measurement errors and selective biases[3]. ROI was completed by 2 doctors. For the region to which the 2 medical practitioners hold different views, they merely engaged in joint discussion to reach an agreement but failed to adopt a statistical method to objectively evaluate the ROI the other doctor outlined[4]. The analyses performed were only combined with FS-T2WI images. They should've been combined with FS-T1WI, DWI and IVIM sequences in later section to implement comparative analysis[5]. Future studies are supposed to include more clinical parameters.

Conclusions

To sum up, radiomics analysis of the FS-T2WI sequence in routine MR images can be performed to determine the decrease extent of glomerular filtration rate in ADPKD patients, able to differentiate patients with GFR $\geq$ 60 mL/min per 1.73 m^2 (including CKD1 and CKD2 phases) from patients with GFR < 60 mL/min per 1.73 m^2 (CKD3 and advanced phases). Among the models constructed with image data and patient clinical information, LR model showed the best diagnostic potency. Thanks to these advantages, radiomics techniques are expected to be a strong supplement to eGFR and htTKV, two extant diagnostic indicators for ADPKD. The coupling application of image data features-clinical variables-machine learning model (LR) presented a better performance in patient classification and individual prognosis, compared with traditional diagnosing approaches. Radiomics analysis harbors a prominent future in this era of precision medicine. It is hopeful to introduce a new dimension for ADPKD treatment. However, on its way to clinical application there are plenty of challenges, which require research with a large scale of disease cases.

Conflict of Interest

The Authors declare that they have no conflict of interests.

References

1) Xue C, Zhou CC, Wu M, Mei CL. The clinical manifestation and management of autosomal dominant polycystic kidney disease in China. Kidney Dis (Basel) 2016; 2: 111-119.

2) Irazabal MV, Torres VE. Total kidney volume and autosomal dominant polycystic kidney disease: a long-standing relationship. Am J Nephrol 2018; 48: 65-66.

3) Grantham JJ, Mulamalla S, Swenson-Fields KI. Why kidneys fail in autosomal dominant polycystic kidney disease. Nat Rev Nephrol 2011; 7: 556-566.

4) Perrone RD, Mouksassi MS, Romero K, Czerwiec FS, Chapman AB, Gitomer BY, Torres VE, Miskulin DC, Broadbent S, Marier JF. Total kidney volume is a prognostic biomarker of renal function decline and progression to end-stage renal disease in patients with autosomal dominant polycystic kidney disease. Kidney Int Rep 2017; 2: 442-450.

5) Torres VE, Chapman AB, Devuyst O, Gansevoort RT, Grantham JJ, Higashihara E, Perrone RD, Krasa HB, Ouyang J, Czerwiec FS. Tolvaptan in patients with autosomal dominant polycystic kidney disease. N Engl J Med 2012; 367: 2407-2418.
6) Irazabal MV, Rangel LJ, Bergstralh EJ, Osborn SL, Harmon AJ, Sundsbak JL, Bae KT, Chapman AB, Grantham JJ, Mrug M, Hogan MC, El-Zoghby ZM, Harris PC, Erickson BJ, King BF, Torres VE. Imaging classification of autosomal dominant polycystic kidney disease: a simple model for selecting patients for clinical trials. J Am Soc Nephrol 2015; 26: 160-172.
7) Torres VE, Harris PC, Pirson Y. Autosomal dominant polycystic kidney disease. Lancet 2007; 369: 1287-1301.
8) Alam A, Dahl NK, Lipschutz JH, Rossetti S, Smith P, Sapir D, Weinstein J, McFarlane P, Bichet DG. Total kidney volume in autosomal dominant polycystic kidney disease: a biomarker of disease progression and therapeutic efficacy. Am J Kidney Dis 2015; 66: 564-576.
9) Thoeny HC, De Keyzer F, Oyen RH, Peeters RR. Diffusion-weighted MR imaging of kidneys in healthy volunteers and patients with parenchymal diseases: initial experience. Radiology 2005; 235: 911-917.
10) Chandarana H, Lee VS, Hecht E, Taouli B, Sigmund EE. Comparison of biexponential and monoexponential model of diffusion weighted imaging in evaluation of renal lesions: preliminary experience. Invest Radiol 2011; 46: 285-291.
11) Li LP, Halter S, Prasad PV. Blood oxygen level-dependent MR imaging of the kidneys. Magn Reson Imaging Clin N Am 2008; 16: 613-625.
12) Castellano G, Bonilha L, Li LM, Cendes F. Texture analysis of medical images. Clin Radiol 2004; 59: 1061-1069.
13) Li Z, Mao Y, Huang W, Li H, Zhu J, Li W, Li B. Texture-based classification of different single liver lesion based on SPAIR T2W MRI images. BMC Med Imaging 2017; 17: 42.
14) Nie K, Shi L, Chen Q, Hu X, Jabbour SK, Yue N, Niu T, Sun X. Rectal cancer: assessment of neoadjuvant chemoradiation outcome based on radiomics of multiparametric MRI. Clin Cancer Res 2016; 22: 5256-5264.
15) Castellano G, Bonilha L, Li LM, Cendes F. Texture analysis of medical images. Clin Radiol 2004; 59: 1061-1069.
16) Kunimatsu A, Kunimatsu N, Kamiya K, Watadani T, Mori H, Abe O. Comparison between Glioblastoma and Primary Central Nervous System Lymphoma Using MR Image-based Texture Analysis. Magn Reson Med Sci 2018; 17: 50-57.
17) Nakajo M, Jinguji M, Nakabeppu Y, Nakajo M, Higashi R, Fukukura Y, Sasaki K, Uchikado Y, Natsugoe S, Yoshiura T. Texture analysis of (18) F-FDG PET/CT to predict tumour response and prognosis of patients with esophageal cancer treated by chemoradiotherapy. Eur J Nucl Med Mol Imaging 2017; 44: 206-214.
18) Yagi T, Yamazaki M, Ohashi R, Ogawa R, Ishikawa H, Yoshimura N, Tsuchida M, Ajioka Y, Aoyama H. HRCT texture analysis for pure or part-solid ground-glass nodules: distinguishability of adenocarcinoma in situ or minimally invasive adenocarcinoma from invasive adenocarcinoma. Jpn J Radiol 2018; 36: 113-121.
19) Horie S. Sensing the texture of imaging, a new biomarker of polycystic kidney disease. Kidney Int 2017; 92: 1044-1045.
20) Yu A, Shen C, Landsittel DP, Harris PC, Torres VE, Mrug M, Bae KT, Grantham JJ, Rahbari-Oskoui FF, Flessner MF, Bennett WM, Chapman AB. Baseline total kidney volume and the rate of kidney growth are associated with chronic kidney disease progression in Autosomal Dominant Polycystic Kidney Disease. Kidney Int 2018; 93: 691-699.
21) Perico N, Antiga L, Caroli A, Ruggenenti P, Fasolini G, Cafaro M, Ondei P, Rubis N, Diadei O, Gherardi G, Prandini S, Panozo A, Bravo RF, Carminati S, De Leon FR, Gaspari F, Cortinovis M, Motterlini N, Ene-Iordache B, Remuzzi A, Remuzzi G. Sirolimus therapy to halt the progression of ADPKD. J Am Soc Nephrol 2010; 21: 1031-1040.
22) Torres VE, Chapman AB, Devuyst O, Gansevoort RT, Perrone RD, Dandurand A, Ouyang J, Czerwiec FS, Blais JD. Multicenter, open-label, extension trial to evaluate the long-term efficacy and safety of early versus delayed treatment with tolvaptan in autosomal dominant polycystic kidney disease: the TEMPO 4:4 Trial. Nephrol Dial Transplant 2017; 32: 1262.
23) Kline TL, Korfiatis P, Edwards ME, Bae KT, Yu A, Chapman AB, Mrug M, Grantham JJ, Landsittel D, Bennett WM, King BF, Harris PC, Torres VE, Erickson BJ. Image texture features predict renal function decline in patients with autosomal dominant polycystic kidney disease. Kidney Int 2017; 92: 1206-1216.
24) Chapman AB, Guay-Woodford LM, Grantham JJ, Torres VE, Bae KT, Baumgarten DA, Kenney PJ, King BJ, Glockner JF, Wetzel LH, Brummer ME, O'Neill WC, Robbin ML, Bennett WM, Klahr S, Hirschman GH, Kimmel PL, Thompson PA, Miller JP. Renal structure in early autosomal-dominant polycystic kidney disease (ADPKD): The Consortium for Radiologic Imaging Studies of Polycystic Kidney Disease (CRISP) cohort. Kidney Int 2003; 64: 1035-1045.
25) Li Z, Mao Y, Huang W, Li H, Zhu J, Li W, Li B. Texture-based classification of different single liver lesion based on SPAIR T2W MRI images. Bmc Med Imaging 2017; 17: 42.
26) Gansevoort RT, Arici M, Benzing T, Birn H, Capasso G, Covic A, Devuyst O, Drechsler C, Eckardt KU, Emma F, Knebelmann B, Le Meur Y,

Massy ZA, Ong AC, Ortiz A, Schaefer F, Torra R, Vanholder R, Wiecek A, Zoccali C, Van Biesen W. Recommendations for the use of tolvaptan in autosomal dominant polycystic kidney disease: a position statement on behalf of the ERA-EDTA Working Groups on Inherited Kidney Disorders and European Renal Best Practice. Nephrol Dial Transplant 2016; 31: 337-348.

27) Kwak JT, Xu S, Wood BJ, Turkbey B, Choyke PL, Pinto PA, Wang S, Summers RM. Automated prostate cancer detection using T2-weighted and high-b-value diffusion-weighted magnetic resonance imaging. Med Phys 2015; 42: 2368-2378.

28) Wu J, Zhu Q, Zhu W, Chen W. CT and MRI imaging features and long-term follow-up of adult Wilms' tumor. Acta Radiol 2016; 57: 894-900.

29) Konda SD, Aref M, Wang S, Brechbiel M, Wiener EC. Specific targeting of folate-dendrimer MRI contrast agents to the high affinity folate receptor expressed in ovarian tumor xenografts. MAGMA 2001; 12: 104-113.

30) Eftekhar B, Mohammad K, Ardebili HE, Ghodsi M, Ketabchi E. Comparison of artificial neural network and logistic regression models for prediction of mortality in head trauma based on initial clinical data. BMC Med Inform Decis Mak 2005; 5: 3.